MAGNITUDE-YIELD AND TRAVEL-TIME CALIBRATION OF NORTHERN EURASIA USING DEEP SEISMIC SOUNDING DATASETS

Igor B. Morozov[1], W. Scott Phillips[2], and Igor. N. Kadurin[3]

University of Saskatchewan[1], Los Alamos National Laboratory[2], and Center GEON[3]

Sponsored by National Nuclear Security Administration
Office of Nonproliferation Research and Engineering
Office of Defense Nuclear Nonproliferation

Contract Nos. DE-FC52-05NA26609[1] and W-7405-ENG-36[2]

ABSTRACT

This study continues our analysis of digital seismograms from chemical and peaceful nuclear explosions (PNEs) of the Russian Deep Seismic Sounding (DSS) program that have recently become available. In this new project, we are extending this analysis to

- Obtaining ground truth source parameters (charge types, sizes, and other relevant information) of ~500 chemical explosions used in 11 major projects of the DSS program;
- Obtaining and digitizing regional and local earthquakes recorded by the DSS PNE profiles for their use as empirical Green's functions in coda magnitude calibration;
- Coda magnitude analysis for DSS chemical and nuclear explosions;
- Derivation of empirical magnitude (apparent coda source spectra) yield relationships for small (m_b ~1-3) explosion events in Northern Eurasia;
- Study of transportability of the coda source-yield relationship over a broad area and a variety of emplacement conditions based on PNE data and extrapolating the relationship to smaller, chemical yields;
- Examination of the variability of the derived coda calibration parameters, attenuation in particular, along and across the profiles; correlating this variability with geology and tectonics of the area;
- Derivation of a P-wave travel-time calibration model for Northern Eurasia with an unusually well constrained and detailed crustal and uppermost mantle structure based on the chemical explosion data. Using this model, derive sample Source Specific Station corrections (SSSC) for an IMS station (e.g., BRVK) and developing a methodology for its enhancement, and comparing with previous SSSC to assess importance of additional data.

As a result of this effort, we plan to produce a large calibration dataset of stable magnitudes and test magnitude-yield relations for a broad, largely aseismic, and critical portion of Northern Eurasia. Coda calibration will bridge the gap between central Asia and the European Arctic and provide additional calibration information to further work in that area.

OBJECTIVES

From mid-1970s to 1990, Russian scientists carried out an extensive program for DSS of the territory of this the Soviet Union. The program resulted in the acquisition of a network of densely sampled, long-range, three-component profiles using large conventional and peaceful nuclear explosions (PNEs). Currently, an effort (sponsored by AFRL contract DTRA01-01-C-0081 and NSF Grant EAR-0092744) for digitizing these datasets and preserving them in modern digital formats in IRIS (Incorporated Research Institutions for Seismology) and AFRL is underway, with 22 PNEs and 522 chemical explosions archived to date. DSS PNE profiles covered much of the aseismic parts of Northern Eurasia and are now receiving growing attention in their application to seismic calibration and nuclear test monitoring in Northern Asia. In this new project, we plan to derive two types of new calibration information from these datasets

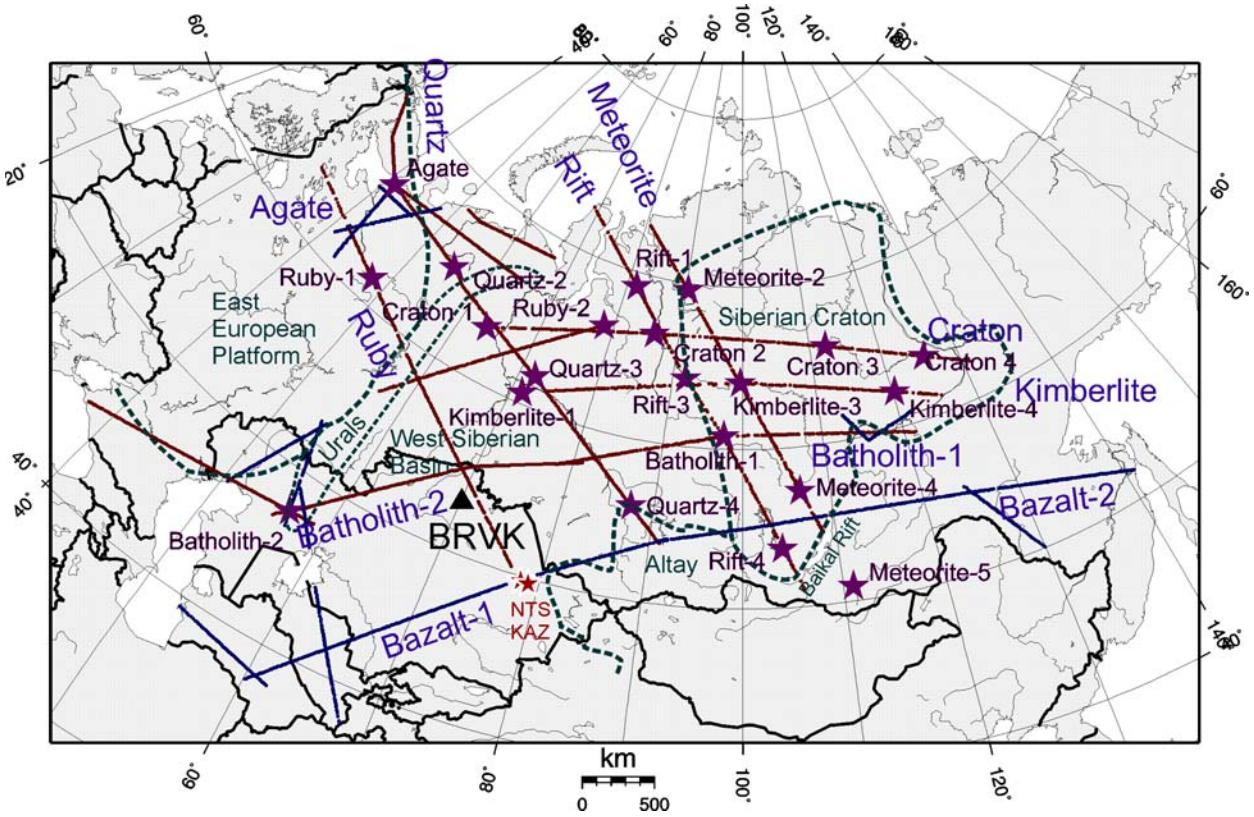

Figure 1. Location map of DSS PNE projects of this project. Projects are labeled in blue, and labeled purple stars show the PNEs. The dataset also includes two Semipalatinsk nuclear test site explosions (red). Parameters of the PNEs were reported by Sultanov et al (1999). Major tectonic units are indicated in green. Small brown circles (mostly appearing as lines at station spacing of 10-15 km) are PNE recording stations, and blue circles are chemical-explosion recording stations. Each profile also contains from 30 to 150 chemical explosions. Borovoye IMS station is also indicated (BRVK).

The primary objective of this study is to derive stable and transportable regional magnitudes of smaller events. The importance of using chemical explosions would be to study the magnitude (seismic amplitude corrected for distance and attenuation) versus yield relationships for smaller events and over a broad area. Smaller events of $m_b < 3.0$ are critical for nuclear test monitoring yet they are poorly represented in cratonic parts of Northern Eurasia, where most of calibration data come from PNEs and large mining explosions (Conrad et al., 2001). Depending on their explosion efficiency; DSS chemical shots should range, in terms of coda magnitudes, from ~1.0 to ~2.5 (Brocher, 2003). As the shots were designed for refraction seismic profiling (e.g., many of them shot in water reservoirs), they are likely to lie on the higher-efficiency end of the magnitude spectrum. Therefore, utilizing the chemical DSS datasets should help extrapolating magnitude calibration results to smaller yields.

Use of redundant recordings from over 500 shots should allow us to better account for path and site terms and derive coda magnitude estimates. High-efficiency DSS shots, even those conducted in water, are likely to produce strong *S* waves created through mode conversions on the base of the weathering layer or reservoir bottom. We will examine the amplitudes and the resulting magnitudes for stability and transportability, and also collect a comprehensive database on phase amplitude ratios at local distances. The coda work will be performed using standard techniques common to the NNSA laboratories that will allow integration with the Knowledge Base, as well as direct comparison with yield studies in other regions to test transportability. A useful side benefit of the work will be an extension of absolute coda calibration from central Asia to the European Arctic, where coda calibration performed by the Lawrence Livermore National Laboratory (LLNL) group relies on a small number of reference earthquakes to obtain absolute levels.

Improvement of travel-time calibration of the region is the second key objective of this research. Several thousand reliable travel-time picks from chemical shots along the DSS PNE lines (Figure 1) will further constrain the crustal velocities, which can then be incorporated into the Source Specific Station Correction (SSSC) tables used for accurate event locations. Improved SSSCs could be derived by incorporation of the chemical-explosion *P*- and *S*-wave travel times into regionalized travel-time models (e.g., Conrad et al., 2001) or into the 3-D apparent-velocity models derived in our recent analysis of the DSS PNEs (Morozov et al., 2005). In addition, based on the detailed, reversed travel-time coverage of the crust along the profiles, we will derive statistical models of the *P*-wave travel-times in the region. Such travel-time statistics could be incorporated into kriging used for IMS station calibration.

RESEARCH ACCOMPLISHED

As the project is in its initial stage, we summarize the key planned approaches, and results of preliminary investigations below.

1) Coda calibration

Coda magnitudes have significantly improved stability (by a factor of 3-5 in interstation scatters of magnitude estimates; Mayeda et al., 2003) compared to body-wave and short-window coda magnitudes. For this reason, we will emphasize coda calibration as our primary approach to source spectra and magnitude estimation. However, apart from the "coda modeling" step below, the following discussion also applies to body-wave amplitudes, which can be treated similarly.

Based on various assumptions about the stochastic properties of the crust and the nature of coda waves, several coda models have been proposed (e.g., Aki and Chouet, 1975; Sato and Fehler, 1998). However, in practice, with virtually any coda model, additional *ad hoc* distance and spectral corrections are required to obtain earthquake moment-rate spectra (Mayeda and Walter, 1996; Phillips et al., 2004). We will thus rely on an empirical procedure endeavoring to capture the key features of coda scattering phenomena by specifying a set of parameters that are adjusted by (typically) nonlinear fitting procedures. Such a coda calibration method is based on the following coda envelope model (modified after Mayeda et al., 2003):

$$A(t, f, r) = W_0(f) S(f) P(r, f) A_{shape}(t - t_0), \qquad (1)$$

where $W_0(f)$ is the *S*-wave source amplitude, $S(f)$ is the recording site response including the S-wave to coda scattering transfer function, $P(f,r)$ represents the effects of propagation (spreading, scattering, and absorption), $A_{shape}(t\text{-}t0,f,r)$ is the temporal signal shape function (coda, or a broadening pulse for body waves), t is the time, t_0 is the time of the *S*-wave peak envelope at the receiver, r is the source-receiver distance, and f is the frequency.

The procedure to separate the various factors in the expression above includes (1) band-pass filtering to form narrowband envelopes; (2) measurement of the moveout velocities of the peak S-, Lg- or surface-wave amplitudes (depending on band); (3) fitting empirical synthetics for the observed shapes of coda envelopes; (4) empirical distance corrections, including tomography for laterally varying attenuation; (5) empirical Green's function corrections to obtain relative spectral shapes; and (6) tying the relative spectra to independently determined seismic moment. This procedure accounts for propagation, site, differing coda composition (Lg, surface waves) in each band, and the efficiency of coda generation. As a result, the method provides stable and unbiased spectra and derived magnitude estimates (Mayeda et al., 2003). Results are the moment rate spectra for earthquakes and the apparent coda source spectra for explosions, with the term "apparent" indicating the possible inclusion of near source effects, including coupling, shear transfer function and near source path that are not experienced by the earthquakes used to calibrate the coda.

We will apply standard National Nuclear Security Administration (NNSA) coda calibration techniques in order to remain consistent with work performed by other laboratories (e.g., Mayeda et al., 2003). However, several critical steps deserve additional attention in the coda calibration procedure above and the dense sampling of the DSS data sets should prove valuable. For example, the measurement of the moveout velocity of the peak (step 2) as a function of distance, is typically performed on manually determined peak times that show significant scatter. This scatter could result from the broad peaks that are occasionally observed, or from systematic propagation factors, such as variable velocity or variable modal composition of the peak arrival along different paths. The dense spacing of receivers along a common path will allow us to watch the development of envelope peaks with distance, and whether or not the variation is random or systematic will be quickly obvious. This could lead to application of two-dimensional group velocity maps for determining envelope peaks as an enhancement to current coda techniques.

In addition, the coda shape modeling (step 3) could be critical in the derivation of the "true" (pre-coda) *S*-wave amplitude (Morozov and Smithson, 2000). Several heuristic coda decay models can be employed, such as a superposition of power and exponential decays (the standard NNSA coda shape model, Mayeda et al., 2003):

$$A_{shape}(t) \equiv A_{coda}(t) \propto H(t) t^{-\gamma(r,f)} e^{-b(r,f)t}, \tag{2}$$

where γ and b control the short and long time range, frequency- and distance-dependent coda amplitude decay behavior, respectively, and $H()$ is the Heaviside step function. For the dependence of γ on distance, Mayeda et al. (2003) used a hyperbolic three-parameter expression,

$$\gamma(r) = \gamma_0 - \frac{\gamma_1}{\gamma_2 + r}, \tag{3}$$

and a similar expression for b. An undesirable property of the form $A_{coda}(t)$ above is the trade-off between γ and b making its interpretation and formal least-squares fitting problematic. Morozov and Smithson (2000) used another empirical model representing the record as a superposition of an *S*-wave onset of finite duration and its exponential coda (Figure 2):

$$P(t - t^0) = \begin{cases} 0, & t < t^0, \\ \lambda P^0 \tau \exp\left[-\beta(t - t^0)\right], & t \geq t^0. \end{cases} \tag{4}$$

We will try the above, or other similar forms in our analysis. This will better separate direct wave and coda portions of the envelope, which is currently done by specifying *ad hoc* minimum offset start times for all distances for a given band in the coda calibration.

Distance correction (step 4 above) is critical for obtaining low interstation magnitude scatter and consequently (eventually) stable discriminants. Many heuristic dependencies for distance dependence of *S*-wave amplitudes can be used, such as (Mayeda et al., 2003),

$$P(r, f) = \frac{1}{1 + \left(\frac{r}{R_0(f)}\right)^{p(f)}}, \tag{5}$$

where R_0 is the characteristic distance at which the which the amplitude starts to decrease (typically, 20-100 km), and p is the far-offset effective attenuation factor (including geometrical spreading and other effects). In another model, the path effect is decomposed into a combination of predefined geometrical spreading and an attenuation-related path integral (e.g. Phillips et al., 2004),

$$P(r, f) = G(r) e^{-\int \frac{\pi f}{vQ} dl} \tag{6}$$

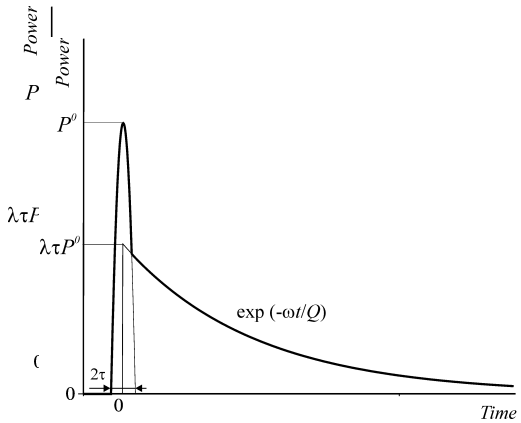

Figure 2. Coda model by Morozov and Smithson (2000). The trace power envelope is represented by a superposition of a finite-bandwidth primary pulse of power P_0 and duration 2τ, followed by its coda of relative amplitude $\lambda\tau$.

where G represents geometrical spreading. Instead of the (R_0,p) parameters above, this path correction for all paths is characterized by a common spatial grid of values of $\{Q(f)\}$. This tomographic approximation, adopted at LANL, is preferable if significant variation of regional extents of coverage (such as between the PNEs and chemical shots), or significant spatial or azimuthal variations are expected, as in this study. As an additional possibility, parameters controlling the frequency-independent geometric spreading $G(r)$ could also be included into the tomography. The dense DSS sampling at long and short distances, including chemical shots at short distances, will allow the separation of spreading and attenuation effects.

The strength of DSS datasets is in their linearity and high recording density (10-15 km station spacings) with numerous sources recorded by groups of stations. At the same time, DSS absolute recording amplitudes may have not been well calibrated, in combination with unknown site and path effects. Utilizing the redundancy of recordings, this lack of absolute calibration could be overcome by forming distance-, coda shape-, and site response-corrected source amplitudes:

$$W_0(f) = \frac{A(t, f, r)}{S(f)P(r, f)A_{coda}(t - t_0)}, \qquad (7)$$

for every frequency f. In this expression, $S(f)$ is associated with every receiver, $W_0(f)$ – with every shot, and $P(r,f)$ is controlled by the parameters $\{Q\}$ varying along the profile. Finally, the requirement:

$$W_0(f) = const$$

for all records from the same shot, leads to an overdetermined (tomographic) inverse problem.

The long-range PNE and short-range chemical path effects may or may not be consistent with each other. Physically, the question is whether or not crustal *S* and *Lg* and their associated coda sample the same portions (depths) of the crust. If they do, we could use one *Q* model along the profile for all data, if not, we will have to calibrate the chemical-shot (presumably shallow) and PNE ("deep") *Q* models separately. This could be an important result of this study, giving us further insight into coda calibration for a wide range of distances that will be difficult to obtain from traditional data sets.

The objective of the final coda calibration steps (5-6) above is to compensate for the frequency-dependent site effects, including the *S*-wave to coda scattering amplitudes and shift to absolute units. This is normally achieved by using small earthquakes as empirical Green's functions and large reference events with independently determined moments. For this study, we will use several PNEs recorded at permanent stations and whose apparent coda source spectra have been obtained as part of the LANL coda calibration effort. As an example, from our preliminary investigations, records from PNEs Meteorite-2, 3, and 4, Kimberlite-3, Batholith-1, Rift-3 and 4, Quartz-4, and Ruby-1 (Figure 1) are present in the Borovoye station archive available at LANL. Additionally, PNE profiles recorded a number of local and regional earthquakes that could also be used to calibrate, or at minimum, to validate

the absolute source spectra. Digitization and obtaining these earthquake records together with the corresponding location and magnitude information is an important part of GEON's contribution to the present project. This will provide redundancy to a critical calibration step.

Magnitude-yield analysis will be used to relate the seismic efficiency to source conditions (Brocher, 2003). According to our present knowledge, many of the chemical shots, particularly in the hard-to-access areas of Siberia, were conducted in lakes or other water reservoirs. This mode of detonation results in the best source coupling, and thus the resulting events should fall on the higher-magnitude envelope in the yield-magnitude cross-plots (Brocher, 2003). For purposes of studying yield transportability, we will simply compare apparent coda source amplitude in various bands to yield, rather than compare magnitude to yield.

2) Travel-time mapping and regional reference model for building SSSCs

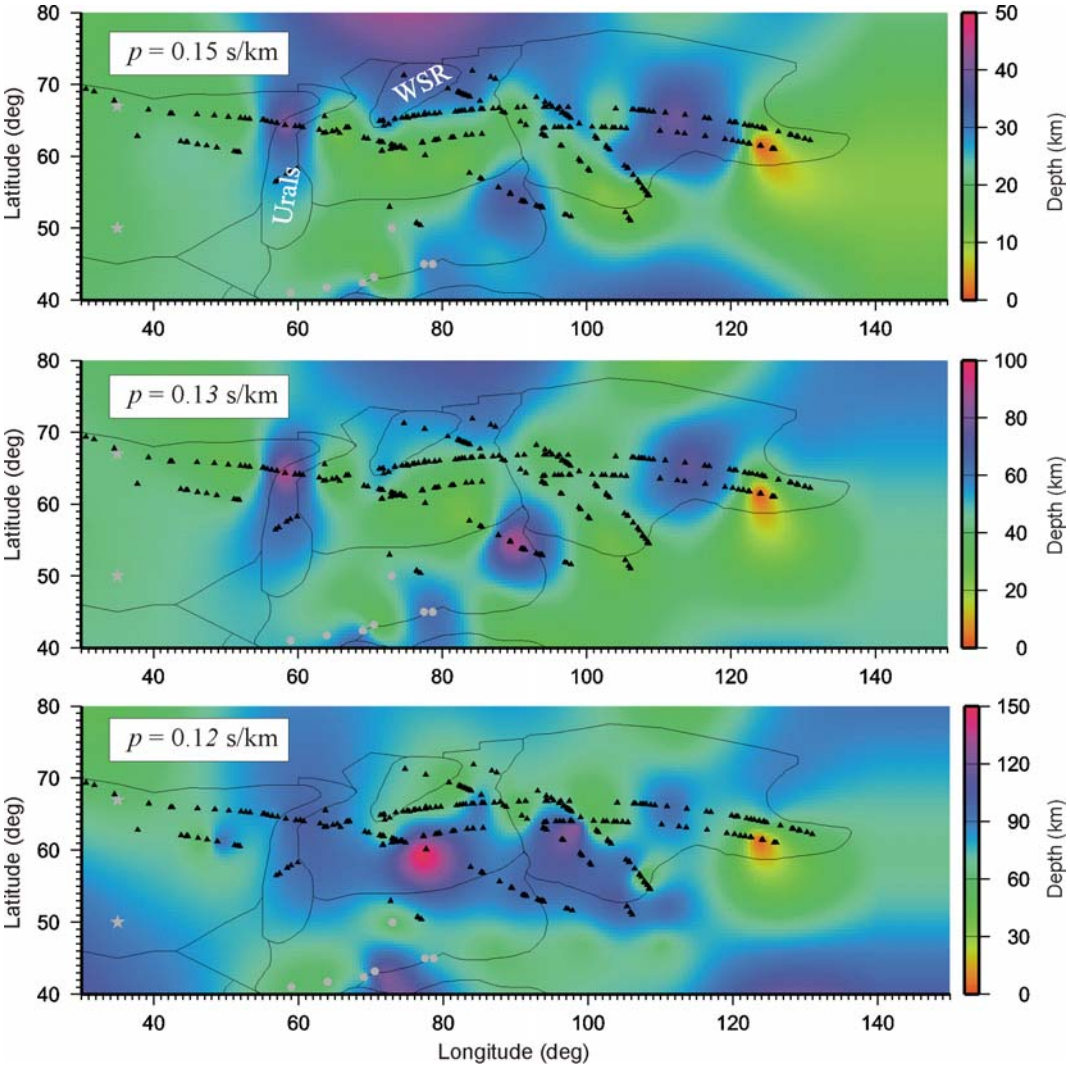

Figure 3. Slices at three values of apparent slowness, *p*, through the 3-D travel-time calibration model, as labeled. The model uses only DSS PNE times constrained with several additional regional travel-time curves (with Baltic Shield and Kazakhstan) and was derived in a straightforward, single-pass procedure (cf. Morozov et al. 2005). In this study, travel times picked from ~500 additional DSS chemical explosion records will greatly improve the shallow part of this model.

Depending on the way travel times are parameterized and associated with surface locations, numerous interpolation schemes can be devised for them, and it is important to choose the one reflecting the fundamental character of the surface-to-surface refraction travel-time problem. In addition, an optimal interpolation scheme should include scalability allowing incorporation of additional data as it becomes available and thereby attaining high accuracy and detail of travel-time prediction. In traditional travel-time regionalization, the regional travel-time dependencies are usually combined using a heuristic interpolation rule, such as (Bondár et al., 2001; Yang et al., 2001):

$$t(S,R) = \frac{\sum_i L_i t_i(d_{SR})}{d_{SR}}, \qquad (8)$$

where S is the source, R is the receiver (both assumed to be located close to the surface), L_i is the length of the great-arc segment connecting S and R and lying within the i-th region, and $d_{SR} = \sum_i L_i$ is the total source-receiver distance. With this rule, the scalability criterion above cannot be met, principally because the travel times vary systematically with offsets and cannot be directly associated with locations. In consequence, the rule above can only be used (and works reasonably well) when the number of regions is small, offsets are large, and crustal variability does not need to be reproduced. However, with the detailed travel times available from additional PNEs and hundreds of DSS chemical explosions distributed over the area (Figure 1), we would need a more accurate and detailed interpolation scheme, and founded on fundamental physical principles of refraction.

Our "regionless" calibration scheme results in a continuous, 3-D travel-time "cube" and was successfully applied to DSS PNE travel times (Morozov et al., 2005). The idea of the method is as follows. Unlike travel times determined along extended subsurface paths, the velocity structure *is* naturally associated with geographical and depth coordinates and therefore it can be spatially interpolated. Thus, by contrast to the formula above, our travel-time mapping is performed through interpolation of an effective "velocity structure" rather than of the travel times themselves. Schematically, this method can be presented as a series of three transformations:

$$t(r)|_{L_i} \xrightarrow{1)\ \tau-p} \tau(p)|_{L_i} \xrightarrow{2)\ HWT} \Delta z(p)|_{L_i} \xrightarrow{3)\ Interpolation} \Delta z(p)|_{(x,y)} \qquad (9)$$

Here, i=1…N counts the observed travel-time curves, L_i is the great arc connecting the source and receiver, r is the range (source-receiver distance), approximated along the great arc, $t(r)$ is the observed travel time, p is the ray parameter, $\tau(p)$ is the delay (intercept) time (e.g., Buland and Chapman, 1983), x and y are the spatial (geographic) coordinates, and Δz is the layer thickness in the resulting 3-D apparent-velocity model. The Herglotz-Wiechert transform (HWT) is used to encode the $\tau(p)$ dependences into the equivalent "apparent velocity columns" $\Delta z(p)$ that are further spatially interpolated to yield a 3-D model cube, $\Delta z(p|x,y)$ (Figure 3).

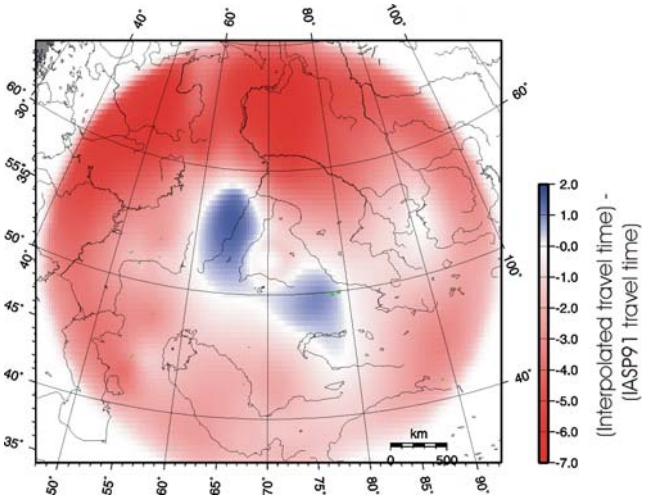

Figure 4. SSSC for station BRVK (Kazakhstan) predicted from DSS PNE travel times alone (Figure 3).

The essential improvement offered by this method as compared to traditional regionalization is its ability to accommodate realistic velocity structure and any volume of input data, similarly to 3-D velocity tomography. On the other hand, compared to tomography, this method is simple, free from uncertainties of the inversion, performed in one "downward" pass and does not require regularization. Finally, using a simple 1.5D ray tracing, this model can be used to quickly generate the Source-Specific Station Corrections (SSSC) for any location, as illustrated in Figure 4 for station BRVK.

Similar to the coda calibration model above (Figure 2), the 1.5D $\tau(p)$ parameterization of the first-arrival travel times separates the contributions from the near- (site terms) and long-range (path terms) propagation. Without such a separation in the previous work, fine-scale variations that are really site effects may have been effectively mapped into the deeper structures.

In this study, we will use the first-arrival travel times picked from all chemical explosions to augment the apparent-velocity model of Northern Eurasia (Figure 3). Even with limited sampling from 19 PNEs, the model already reproduces the key characteristics of the regional travel times in the area. With addition of several hundred of travel time curves from the chemical DSS shots, this model will account for the crustal variability and reproduce the associated travel times significantly more accurately.

Even after its enhancement from all DSS travel times, the travel-time model in Figure 3 would still not account for the near-source and receiver effects in the vicinities of the sources and receivers not included in its derivation. However, the model already represents a far better regional reference model then IASP91, and it can be additional fine-tuned by its use as a regional background and utilizing additional ground truth events in standard SSSC calibration procedures, such as kriging (Myers and Schultz, 2000). Note that the analysis of detailed DSS travel times could be the key source of quantitative information on the travel-time correlation functions for kriging, as described below.

Testing SSSC sensitivity to additional data

To assess the improvement from the use of detailed chemical-shot travel times, we will compute the travel times from all the available DSS shots to a selected point in the model, such as the IMS station Borovoye, and subtract from them the travel times predicted by the IASP91 model, by the existing SSSCs (such as derived by the Group II Location Calibration Consortium; Conrad et al., 2001), or by our current PNE-based SSSC (Figure 4). The resulting distributions of travel-time residuals would provide quantitative estimates of the significance of short-scale (~50-100-km) crustal variability for travel-time prediction. These estimates would be further developed in much more comprehensive statistical sampling of SSSC uncertainty.

Statistical modeling of SSSC travel-time variability

The 3-D apparent-velocity travel-time model above (Figure 3) has the ability to correctly separate the shallow (short-range) and deep (long-range) travel time patterns and also to incorporate the complete structural complexity of the region. Its resolution will only be limited by the available travel-time data concentrated along the linear DSS profiles (Figure 1). In the broader area between and outside the profiles, no detailed travel-time information is available yet a good guidance on the main features of crustal structure is still available. In order to assess the potential effects of such imperfectly known crustal and upper-mantle heterogeneity on the resulting SSSCs, we will utilize the following statistical sampling approach.

First, for each profile, we will extract its corresponding the $\Delta z(p|x,y)$ model out of our 3-D cube and examine its correlation with the available regional summary models (Figure 3). It is likely that in the vicinities of the profiles, the summary models would have to be adjusted to satisfy the detailed DSS travel times. Further, we will extract p- and geographically-dependent statistics of the values $\Delta z(p|x,y)$ (mean values, variances, correlation lengths, or othe parameters of probability distribution functions). This analysis would yield quantitative, ray parameter- dependent (and equivalently, range-dependent) statistical characterization of the spatial variability of the travel times within the region.

With the statistics of the (apparent-)velocity structure characterized, we would use the modified apparent-velocity

models (Figure 3) to build the average crustal structure and simulate a representative number (several thousand) of random realizations. We will further compute SSSC for BRVK, or for other stations of interest, in each of these realizations and compile statistics (mean, autocorrelation functions, and PDFs) on each of them. As a result, this should yield a direct, objective, quantitative, detailed, range and regionally-variant, and (in principle) non-Gaussian, measure of statistical SSSC variability based on the integrated analysis of two comprehensive, complementary datasets.

CONCLUSIONS AND RECOMMENDATIONS

As a result of this effort using a large database of digital seismograms from chemical and PNEs of the DSS program, we will produce a large calibration dataset of stable and transportable magnitudes and magnitude-yield relations for a vast and largely aseismic, which is critical for seismic monitoring in this part of Northern Eurasia. We also anticipate extending absolute coda calibration from central Asia to the European Arctic, where the LLNL coda group could take advantage of the additional calibration information, presumably through constraints from events common to both networks (most likely a PNE recorded at NORSAR).

REFERENCES

Aki, K. and B. Chouet (1975), Origin of coda waves: source, attenuation, and scattering effects, *J. Geophys. Res.* 80: 3: 322-3, 342.

Bondár, I., and V. Ryaboy (1997), Regional travel-time tables for the Baltic Shield region, Technical Report CMR-97/24.

Bondár, I., X. Yang, R. North, and C. Romney (2001), Location calibration data for the CTBT monitoring at the Prototype International Data Center, Pageoph Technical Volumes, Monitoring of the Comprehensive Nuclear Test-Ban Treaty: Source Location, F. Ringdal and B. Kennett (editors), *Pure Appl. Geophys.* 158: 19-34.

Brocher, T. M. (2003), Detonation charge size versus coda magnitude relations in California and Nevada, *Bull. Seism. Soc. Am.* 93: (5), 2089-2105.

Buland, R, and Chapman, C. H. (1983), The computation of seismic travel times, *Bull. Seism. Soc. Am*. 73: 1271-1302.

Conrad, C., Cormier, V., Fisk, M., Ichinose, G., Khalturin, V. I., Kim, W.-Y., Morozov, I., Morozova, E., Richards, P. G., Saikia, C., Shaff, D., and Waldhauser, F., (2001), Annual Technical report: Seismic Location Calibration of 30 International Monitoring System Stations in Eastern Asia, DTRA, Contracts No. DTRA01-00-C-0029, DTRA01-00-C-0031, DTRA01-00-C-0033.

Mayeda, K., A. Hofstetter, J. L. O'Boyle, and W. R. Walter (2003), Stable and transportable regional magnitudes based on coda-derived moment-rate spectra, *Bull. Seism. Soc. Am*. 99: (1), 224-239.

Mayeda, K., and W. R. Walter (1996). Moment, energy, stress drop, and souirce spectra of western United States earthquakes from regional coda envelopes, *J. Geophys. Res.* 101: 11195-11208.

Morozov, I. B., and Smithson, S. B. (2000), Coda of long-range arrivals from nuclear explosions, BSSA, 90, 929-939.

Morozov, I. B., E. A. Morozova, S. B. Smithson, P. G. Richards, V. I. Khalturin, and L. N. Solodilov (2005), 3-D first-arrival regional calibration model of northern Eurasia, *Bull. Seismol. Soc. Am* 95: (3), 951-964, doi:10.1785/0120030173.

Myers, S. C., and Schultz, C. A. (2000), Improving sparse network seismic location with Bayesian kriging and teleseismically constrained calibration events, *Bull. Seism. Soc. Am*. 90: 1, 199-211.

Phillips, W.S., H.J. Patton, S.R. Taylor, H.E. Hartse, and R.E. Randall (2004), Calibration for coda based magnitude and yield, in the *26th Seismic Research Review: Trends in Nuclear Explosion Monitoring*, LA-UR-04-5801, Vol. 1, pp. 449-456.

Sato, H., and M. Fehler (1998), *Seismic Wave Propagation and Scattering in the Heterogeneous Earth*, Springer-Verlag, New York.

Sultanov, D. D., J. R. Murphy, and Kh. D. Rubinstein (1999), A seismic source summary for Soviet Peaceful Nuclear Explosions, *Bull. Seism. Soc. Am*. 89: 640-647.

Yang, X., I. Bondár, K. McLauglin, R. North, and W. Nagy (2001), Path-dependent regional phase travel-time corrections for the International Monitoring system in North America, *Bull. Seism. Soc. Am*. 91: 1831-1850.